Development 140, 2444 (2013) doi:10.1242/dev.098160

CLIPR-59: a protein essential for neuromuscular junction stability during mouse late embryonic development

Aurélie Couesnon, Nicolas Offner, Véronique Bernard, Nathalie Chaverot, Stéphanie Backer, Ariane Dimitrov, Franck Perez, Jordi Molgó and Evelyne Bloch-Gallego

There were two errors published in *Development* **140**, 1583-1593.

On p. 1583, in the first paragraph of the Introduction, the alternative name given for CLIP-115 should be Clip2.

On the same page, the first sentence of the second paragraph of the Introduction should read: *Clip-115* KO mice are also viable…

We apologise to the authors and readers for these mistakes.

Development 140, 1583-1593 (2013) doi:10.1242/dev.087106

CLIPR-59: a protein essential for neuromuscular junction stability during mouse late embryonic development

Aurélie Couesnon[1,2], Nicolas Offner[1,2], Véronique Bernard[3], Nathalie Chaverot[1,2], Stéphanie Backer[1,2], Ariane Dimitrov[4,5], Franck Perez[4,5], Jordi Molgó[6] and Evelyne Bloch-Gallego[1,2,*]

SUMMARY

CLIPR-59 is a new member of the cytoplasmic linker proteins (CLIP) family mainly localized to the trans-Golgi network. We show here that *Clipr-59* expression in mice is restricted to specific pools of neurons, in particular motoneurons (MNs), and progressively increases from embryonic day 12.5 (E12.5) until the first postnatal days. We generated a *Clipr-59* knockout mouse model that presents perinatal lethality due to respiratory defects. Physiological experiments revealed that this altered innervation prevents the normal nerve-elicited contraction of the mutant diaphragm that is reduced both in amplitude and fatigue-resistance at E18.5, despite unaffected functional muscular contractility. Innervation of the mutant diaphragm is not altered until E15.5, but is then partially lost in the most distal parts of the muscle. Ultrastructural observations of neuromuscular junctions (NMJs) in the distal region of the diaphragm reveal a normal organization, but a lower density of nerve terminals capped by terminal Schwann cells in E18.5 mutant when compared with control embryos. Similar defects in NMJ stability, with a hierarchy of severity along the caudo-rostral axis, are also observed in other muscles innervated by facial and spinal MNs in *Clipr-59* mutant mice. *Clipr-59* deficiency therefore affects axon maintenance but not axon guidance toward muscle targets. Thus, CLIPR-59 is involved in the stabilization of specific motor axons at the NMJ during mouse late embryogenesis and its role is crucial for mouse perinatal development.

KEY WORDS: Axon development, Cytoskeleton, Motoneurons, Mouse embryo, Neuromuscular junction, Clip3

INTRODUCTION

Cytoplasmic linker proteins, or CLIPs, define a family of molecules that all include microtubule (MT) binding domains, i.e. their cytoskeleton-associated protein Gly-rich (CAP-Gly) domains (Jaworski et al., 2008). The first member of the family, CLIP-170 (CLIP of 170 kDa; Clip1 – Mouse Genome Informatics), was described as a MT plus end-binding protein that mediates the interactions of endocytic organelles to MTs (Pierre et al., 1992). CLIP-170 is involved in the dynein-dynactin pathway and plays an important role in mitosis (Lansbergen et al., 2004; Wieland et al., 2004). CLIP-170 knockout (KO) mice are viable but males produce sperm with morphological defects (Akhmanova et al., 2005). In mutant mouse primary fibroblasts, MT ends contained less dynactin than those of control cells, but a similar level of CLIP-115 (Clip1 – Mouse Genome Informatics), a close relative of CLIP-170 involved in linking dendritic lamellar bodies to MTs (De Zeeuw et al., 1997). Although disruption of dynein/dynactin inhibits axonal transport in motoneurons (MNs) causing late-onset progressive degeneration (Teuling et al., 2008), no defect has been reported so far in the nervous system of *Clip-170* KO mice.

Clip-170 KO mice are also viable but exhibit a mild growth deficiency and brain abnormalities, particularly hippocampal and motor coordination dysfunctions (Hoogenraad et al., 2002). This phenotype partially mimics Williams syndrome, a rare neurodevelopmental disorder caused by deletion of a region containing several genes, including *CLIP-115*. Moreover, in the absence of *Clip-115*, increased levels of both dynactin and CLIP-170 were observed on MT ends in fibroblasts.

Using a dominant-negative form of CLIP-170 in Chinese hamster ovary cells, CLIP-115 and CLIP-170 were shown to act redundantly as rescue factors via their N-terminal domains. Recently, CLIP-170 and CLIP-115 were both found to be enriched in the growth cones of cultured rat hippocampal neurons, and involved in initial neuronal polarization and axon formation (Neukirchen and Bradke, 2011).

A potential role for another CLIP-related protein in the nervous system has been suggested by the identification of CLIPR-59, or CLIP-related protein of 59 kDa (Clip3 – Mouse Genome Informatics), found to be strongly expressed in the brain. In contrast to CLIP-170 and CLIP-115, CLIPR-59 does not bind MT plus ends. The domains surrounding its two CAP-Gly domains, an N-terminal domain bearing ankyrin repeats and a C-terminal Golgi-targeting domain, inhibit MT interactions (Lallemand-Breitenbach et al., 2004) and the CLIPR-59 MT binding domain alone inhibits MT polymerization. In addition, CLIPR-59 is mainly localized to the *trans*-Golgi network (TGN) (Perez et al., 2002). Dual cysteine palmitoylation enables its recruitment to lipid rafts (Lallemand-Breitenbach et al., 2004) and CLIPR-59 has been proposed to be active at endosome/TGN interface. A role for a TGN-localized MT-binding protein in neuronal cells may be related to the strong need of developing axons to sustain not only polarized intracellular trafficking but also dynamic exocytosis to ensure rapid reorganization of membrane during pathfinding and to establish proper synaptic connections.

In the present work, we therefore studied the function of CLIPR-59 in the development of the nervous system. We show that CLIPR-59 is particularly expressed in MNs, with an increased expression from early to late embryonic development. MNs are highly polarized and differentiated cells that must develop long axons. To

[1]Institut Cochin, Université Paris Descartes, CNRS UMR 8104, Paris, France. [2]Inserm, U1016, Paris, France. [3]INSERM Unité 952, CNRS UMR7224, Université Pierre et Marie Curie, Paris, France. [4]Institut Curie, Paris, France. [5]CNRS UMR144, Paris, France. [6]CNRS, Institut de Neurobiologie Alfred Fessard – FRC2118, Laboratoire de Neurobiologie et Développement UPR3294, Gif sur Yvette, France.

*Author for correspondence (evelyne.bloch-gallego@inserm.fr)

Accepted 30 January 2013

investigate the role of CLIPR-59 *in vivo*, we generated a KO mouse model and found that mutant mice die perinatally from respiratory defects. We detected mis-innervation of the diaphragm by phrenic nerves that arise from cervical MNs, with a degeneration of their distal axon terminals from E15.5 that leads to a lower density of nerve terminals at the NMJ at E18.5 in distal regions of the mutant diaphragm. Similar defects were observed in some muscles innervated by facial and spinal MNs. Our structural and ultrastructural results further indicate that CLIPR-59 depletion is associated with a premature or enhanced retraction of motor axons at the NMJ during mouse embryo development. This suggests that CLIPR-59 plays a crucial role in nerve terminal maintenance, possibly through protein/membrane trafficking or cytoskeleton remodeling at the NMJ.

MATERIALS AND METHODS

Generation of *Clipr-59* mutant mice

Clipr-59 mutant mice were generated at the Mouse Clinical Institute (Strasbourg, France) via insertion of loxP sequences into introns 1 and 5 with a neomycin-resistance gene as a selective marker (Fig. 2A). The targeting vector was electroporated into embryonic stem (ES) cells. Breeding of these mice with mice universally expressing Cre recombinase lead to the generation of mice with one invalidated *Clipr-59* gene (*Clipr-59*$^{+/-}$). *Clipr-59*$^{+/-}$ mice were backcrossed to C57BL/6 mice before intercrossing heterozygous parents to obtain homozygous CLIPR-59-deficient mice (*Clipr-59*$^{-/-}$). DNA was isolated from the tail and used for genotyping with the following primers: GCTCACTGTGC-CCAGAGTTTGAC and GCATAACTCTGAGAGTTTGAGGCC; or AGTAGGACCCTTGAACATGCAACTG and CAGGGTCATTGGG-ATCGAAGAAG. Pregnant Swiss mice were purchased from Janvier Laboratories (Le Genest St Isle, France).

In situ hybridization and MN counts

Cryosections (20 μm) of brain and spinal cord were prepared from mouse embryos and *in situ* hybridization was performed as described previously (Causeret et al., 2004). The *Clipr-59* probe was designed by PCR to precisely encompass the deleted region of CLIPR-59 cDNA in KO mice (nucleotides 374-889 in cDNA). The peripherin probe was kindly provided by M. M. Portier (Moncla et al., 1992). Cell counts was performed at E18.5, as described previously (Backer et al., 2007). Results are means of right and left counts (±s.e.m.) from at least four different embryos of each genotype.

Cell culture and immunolabeling

For primary neuronal cultures, the cervical region of spinal cord was dissected from E12.5 wild-type embryos according to Arce et al. (Arce et al., 1999). Cells were fixed in PBS containing 4% PFA and 10% sucrose for 15 minutes at room temperature. After washing in phosphate-buffered saline solution (PBS), autofluorescence was quenched with 50 mM NH_4Cl (SIGMA) for 20 minutes at room temperature. Cells were rinsed in PBS, blocked in dilution buffer (PBS plus 2% NGS and 0.25% Triton, Sigma) and incubated with primary antibodies: βIII tubulin (TUJ1) (Covance; 1:5000), GM130 (R&D Systems, 1:400) and CLIPR-59 (our preparation; 1:400). The CLIPR-59 antibody was raised in rabbits (Agrobio) against GST-tagged CLIPR-59 protein. Serum was then pre-adsorbed using GST and purified against GST-CLIPR-59.

The secondary antibodies used were: Cy3-coupled anti-rabbit IgG (Jackson ImmunoResearch, 1:1000) and Alexa488-coupled anti-mouse IgG (Invitrogen, 1:1000). Nuclei were stained with DAPI before mounting coverslips in Mowiol. Images of 1024×1024 pixels were taken from a series of optical sections (0.5 μm) using a Zeiss confocal laser-scanning microscope and a 63× objective, using the same microscope settings. The fluorescent signal of CLIPR-59 was quantified in the cell body of MNs using the ImageJ software (100 cells from two independent experiments).

Western blot analysis

Lysates were prepared from different tissues of embryos; 25 μg were processed for western blotting as previously described (Backer et al., 2007) using anti-CLIPR-59 (Abcam, 1:1000), anti-CLIP-170 and anti-CLIP-115 [kindly provided by N. Galjart (Erasmus MC, Rotterdam, The Netherlands), numbers 2360 and 2238, respectively; 1:400], and TUJ1 (1:20,000) for internal normalization. Band intensities of chemiluminescence signal were quantified using the ImageJ software. Results are means (±s.e.m.) from four independent experiments.

Muscle contraction measurements

Hemi-diaphragm preparations with their phrenic nerve dissected from E18.5 embryos were mounted on a force transducer in a chamber containing an oxygenated standard Krebs-Ringer solution. Tension recordings of direct and indirect muscle contraction were performed as described previously (Grandic et al., 2012). Signals from the isometric transducer were amplified, digitized and expressed in Newtons (N). After the experiments, the muscle preparations were fixed with 2% PFA in PBS, and weighted to normalize the data obtained from four mutant and control embryos.

Immunofluorescence on nerve-muscle preparations

Until E14.5, embryos were fixed *in toto* in 4% PFA for 2 hours at room temperature. Embryos from E15.5 to E18.5 were perfused with 2% PFA and post-fixed for 2 hours in 2% PFA at room temperature. Tissues were embedded in PBS containing 10% sucrose and 10% gelatin, and processed into 20 μm cryosections. Autofluorescence was quenched with 50 mM NH_4Cl for 20 minutes at room temperature. The primary antibodies used were anti-peripherin (Millipore; 1:2000), TUJ1 (Covance; 1:5000), anti-S-100 (DAKO, 1:200), anti-MuSK (serum 194T, 1:500) and anti-agrin (serum 205, 1:500), kindly provided by Dr M. A. Ruegg (University of Basel, Switzerland). After extensive washing in PBS, samples were incubated with Cy3-coupled anti-rabbit IgG (Jackson ImmunoResearch, 1:1000), Alexa647-coupled anti-mouse IgG or Alexa488-coupled α-bungarotoxin (Invitrogen, 1:500). Apoptosis was detected in tissue cryosections using a cell death detection kit (Roche Applied Science). Tissues were mounted in Mowiol and analyzed using a Zeiss confocal laser scanning microscope and a 63× objective. For image analysis, series of optical sections of 0.5 μm acquired using the same microscope settings were quantified using the ImageJ software (100 synapses from three control and mutant embryos). For analysis of MuSK and agrin labeling on cryosections, the signal was expressed as total intensity normalized to the synapse area. Data are presented as the mean±s.e.m.

Electron microscopy on E15.5 and E18.5 hemi-diaphragms

Hemi-diaphragms collected from E15.5 and E18.5 embryos were fixed in a 2% PFA/0.2% glutaraldehyde (Sigma) solution in PBS for 2 hours at room temperature. Samples from E15.5 and E18.5 embryos were post-fixed overnight at 4°C in 2% PFA and rinsed in PBS. NMJs were identified detecting nicotinic acetylcholine receptors (nAChRs) with biotinylated α-bungarotoxin (10 μg/ml PBS, 2 hours at 20°C) and streptavidin coupled to gold particles (0.8 nm in diameter; Nanoprobes; 1:100 in PBS/BSA). After postfixation in 1% glutaraldehyde and washing in acetate buffer (0.1 M, pH 7), the signal of the gold immunoparticles was increased using a silver enhancement kit (HQ silver; Nanoprobes) for 2 minutes at room temperature in the dark. Finally, after washing in acetate buffer, sections were treated with 1% osmium, dehydrated and embedded in resin. Ultra-thin sections were cut, stained with lead citrate and examined in a transmission electron microscope (EM 912 Omega, Zeiss) equipped with a LaB6 filament at 80 kV and images were captured with a digital camera (SS-CCD, Veleta 2kx2k). NMJs from three mutant and control embryos were analyzed.

RESULTS

In vivo CLIPR-59 expression during mouse development

According to an EST database (Unigene Cluster *hs.7357*), *ClipR-59* gene expression was ubiquitous but was highest in the nervous system. In northern blot analysis of adult mouse tissues using mouse *Clipr-59* cDNA fragments, high levels of ~4 kb *Clipr-59* transcripts were detected in brain and lower levels in other tissues (pancreas, kidney, skeletal muscle, liver, lung, placenta and heart) [Holly

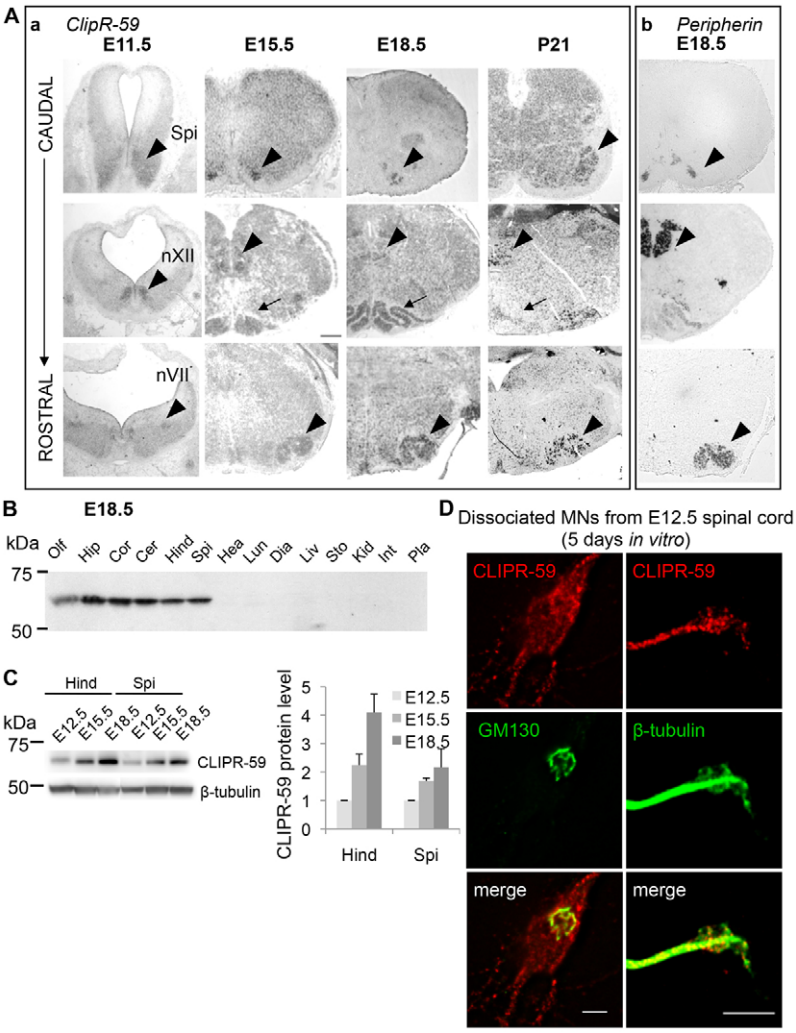

Fig. 1. CLIPR-59 is enriched in embryonic and adult mouse brain and spinal cord. (**A**) *In situ* hybridization on mouse brain and spinal cord cryosections. (a) *Clipr-59* expression increases during embryonic development in several motoneuronal (nVII, nXII; Spi, spinal; arrowhead) and precerebellar nuclei (ION, inferior olive nucleus, arrow). (b) Peripherin is highly expressed at E18.5 in different motoneuronal pools (arrowheads) where *Clipr-59* expression is also detected. (**B**) CLIPR-59 protein levels detected by western blot are high in lysates from different regions of the brain (Olf, olfactory bulb; Hip, hippocampus; Cor, cortex; Cer, cerebellum; Hind, hindbrain) and spinal cord (Spi) of E18.5 mouse embryos, but are very low in lysates from other tissues (Hea, heart; Lun, lung; Dia, diaphragm; Liv, liver; Sto, stomach; Kid, kidney; Int, intestine; Pla, placenta). (**C**) The protein levels of CLIPR-59 increase from E12.5 to E18.5 in both hindbrain and spinal cord lysates. Data are mean±s.e.m. (**D**) CLIPR-59 is localized juxtaposed to the Golgi network labeled with anti-GM130, and along the axon and in the growth cones (see higher magnification) of dissociated spinal motoneurons. Scale bars: 5 μm.

Goodson, personal communication (Notre Dame University, South Bend, IN, USA)] (Perez et al., 2002). Using a systematic bioinformatic approach (Huminiecki et al., 2003), we also found that *Clipr-59* was expressed at its highest levels in the brain compared with its expression levels in other tissues.

Specific expression of *Clipr-59* in the mouse nervous system was further characterized using in situ hybridization with an antisense probe directed against *Clipr-59* mRNA in brain and spinal cord cryosections [control in situ hybridization with a sense probe revealed no signal (data not shown)]. During development, *Clipr-59* mRNA could be detected at low levels as early as E11.5 in the spinal and cranial MNs, including the V, VII, X and XII nuclei (Fig. 1A, arrowheads). The intensity of the mRNA signal increased in MN pools during embryonic development and slightly decreased in the adult (postnatal day 21, P21). Thus, *Clipr-59* expression is finely and not ubiquitously expressed in the nervous system, as MNs show higher mRNA expression than surrounding cells. Peripherin mRNA is present at high levels in motor nuclei of cranial nerves (in particular the V, VII, X and XII nuclei), as well as in ventral horn MNs (Leonard et al., 1988), and accordingly we observed at E18.5 by *in situ* hybridization strong expression of peripherin in motoneuronal pools, where *Clipr-59* signal was detected (Fig. 1B).

Western blot analysis of mouse tissues at E18.5 confirmed that *Clipr-59* was highly expressed in different regions of the brain and spinal cord, but that expression was very low in other tissues, such as lung, heart and diaphragm (Fig. 1B). Moreover, CLIPR-59 protein levels increased progressively between E12.5 and E18.5 in hindbrain and spinal cord extracts (four- and twofold, respectively) (Fig. 1C).

We also examined the intracellular localization of CLIPR-59 in neuronal cells (Fig. 1D). Although only low levels of CLIPR-59 protein could be detected in HeLa cells, immunofluorescence experiments carried out previously in these cells identified the TGN as a principal localization site for CLIPR-59 (Perez et al., 2002). For these experiments, we used a new antibody raised against CLIPR-59 to stain E12.5 primary MNs dissociated either from the facial nucleus (VII) or from ventral spinal cord (cervical region), as *in situ* hybridization and western blot experiments detected high levels of *Clipr-59* expression in these MN pools during mouse development. CLIPR-59 staining in MNs increased by 2.5±0.3-fold from 2 to 5 days *in vitro*, and it appeared concentrated in a tubulovesicular network in the cell body juxtaposed to GM130 staining, but also as punctate staining at the growth cone and to a lesser extent along the axon (Fig. 1D).

CLIPR-59 deficiency in mice and perinatal death

To investigate the role of CLIPR-59 in the mammalian nervous system, mice lacking CLIPR-59 were generated (Fig. 2A). *In situ* hybridization in brain cryosections from E18.5 embryos confirmed the absence of *Clipr-59* expression in homozygous knockout mice (*Clipr-59*$^{-/-}$, data not shown). Moreover, CLIPR-59 protein was not

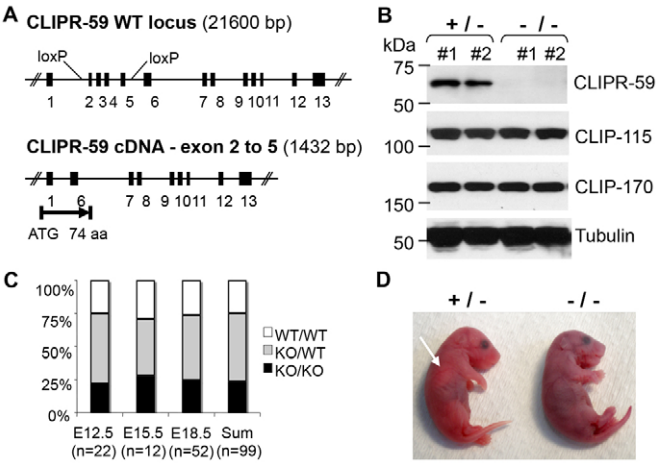

Fig. 2. CLIPR-59-deficient mice die at birth from respiratory failure. (**A**) Schematic representation of the wild-type and recombined CLIPR-59 loci after insertion of loxP sites and excision of exons 2-5 by Cre recombinase. (**B**) CLIPR-59 protein is undetectable by western blot in spinal cord lysates from E18.5 mutants, whereas the levels of CLIP-115 and CLIP-170 are similar to those of controls. (**C**) The genotype ratio in litters from heterozygous mating is Mendelian at different embryonic stages. (**D**) Following Cesarean section of pregnant mice and stimulation of the E18.5 embryos by tail pinching, mutants are never able to breathe, become cyanosed and die. By contrast, control embryos are able to breathe and their open lungs are evident by thoracic transparency (arrow).

detected in spinal cord and cortex lysates from *Clipr-59*$^{-/-}$ E18.5 embryos (Fig. 2B). No effect was observed in the expression of *Clip-170* and *Clip-115* in the spinal cord of *Clipr-59*$^{+/-}$ and *Clipr-59*$^{-/-}$ E18.5 embryos (Fig. 2B).

Clipr-59$^{+/-}$ mice are healthy and fertile but no homozygous mutants were identified at postnatal day 1 (P1) in the ten litters from mated *Clipr-59*$^{+/-}$ mice. However, we observed no prenatal mortality, *Clipr-59*$^{-/-}$ embryos being present in a normal Mendelian ratio at all developmental stages (Fig. 2C), suggesting that CLIPR-59 deletion did not impair *in utero* survival. Therefore, we focused our analysis on E18.5 embryos for all subsequent studies on CLIPR-59-deficient mice.

Upon attempts to resuscitate E18.5 embryos from mated *Clipr-59*$^{+/-}$ mice, only homozygous mutants died shortly after the Cesarean section. Despite exhibiting normal gross morphologies at E18.5, responsiveness to mild pinches on their tails and legs, and having some gasps, *Clipr-59*$^{-/-}$ embryos were unable to expand their lungs and rapidly became cyanosed (Fig. 2D): respiratory failure. As the diaphragm is innervated by phrenic nerves consisting of axons from MNs located in the cervical spinal cord (which strongly express *Clipr-59*), we next analyzed diaphragm innervation in mutant (*Clipr-59*$^{-/-}$) and control (*Clipr-59*$^{+/-}$) embryos.

Normal early development but incomplete innervation pattern of the E18.5 diaphragm in the absence of CLIPR-59

To visualize phrenic nerve arborizations in whole-mounts of diaphragms from E12.5 to E18.5, we labeled the intermediate filament protein peripherin, which is expressed as early as E9.5 in MNs and in peripheral sensory neurons (Duprey and Paulin, 1995). During normal mouse development, axons of the phrenic nerve exit the cervical spinal cord and reach the diaphragm primordium at E12.5. Then each phrenic nerve divides into three main branches: the crural branch that innervates the crus (a muscle not involved in breathing movements), and the dorsal and ventral branches. Whole-mount immunostaining of peripherin indicated no significant differences in the innervation patterns of mutant and control diaphragms at E13.5 and E15.5 (data not shown and Fig. 3A). However, in later developmental stages of mutant embryos, a progressive loss of innervation was observed in the most distal parts of the main phrenic branches, in particular in the ventral region of the diaphragm (Fig. 3B, frame in 3C), and also, albeit with a reduced severity, in the dorsal region of the muscle (arrow in Fig. 3C and supplementary material Fig. S1). By E18.5, the ventral part, and to a lesser extent, the dorsal part of the diaphragm were not innervated in the mutants (Fig. 3C). However, postsynaptic nAChR clusters (labeled with α-bungarotoxin in green) could be observed at the center of the diaphragm muscle from both control and mutant E18.5 embryos (Fig. 3C). The lengths of the primary branches of the phrenic nerve were similar at E15.5 for control and mutant embryos (Fig. 3D), but significantly shorter in mutant embryos at E18.5 (Fig. 3E). In addition, the mean length of the major secondary branches of the right phrenic nerve was significantly longer in mutant than in control embryos at E18.5 (Fig. 3F). However, there was some disparity among individuals of the same genotype.

Analysis of the distribution of nAChR clusters revealed their confinement in a central band of the muscle in both mutant and control diaphragms at all stages between E15.5 and E18.5 (data not shown and Fig. 3C). A slight enlargement of the nAChR band was observed in the aneural part of the mutant diaphragm (frame in Fig. 3C), possibly owing to the loss of presynaptic nerve terminals in this region (Fig. 3G).

Reduced contraction force of the diaphragm from CLIPR-59-deficient embryos at E18.5

As we observed discrete defects in diaphragm innervation in *Clipr-59*$^{-/-}$ embryos and breathing depends primarily on phrenic nerve-diaphragm activity, we next tested the ability of this muscle to contract in nerve/hemi-diaphragm preparations at E18.5. Through nerve stimulation, the maximal twitch tension in mutant hemi-diaphragms was about half of that recorded in control muscles (Fig. 4A). However, when hemi-diaphragms from mutant embryos were directly stimulated, the maximal contraction was not significantly different from that recorded in control muscles. Hence, in the absence of CLIPR-59, the target muscle retains its contractility capacity, whereas phrenic nerve-elicited contraction is greatly impaired. Next, we tested the influence of the stimulation frequency of single phrenic nerve pulses on isometric tension (Fig. 4B). No differences in the frequency-dependence of the nerve-elicited contractions were evident between mutant and control hemi-diaphragms.

We further studied whether isometric tetanic tension could be sustained upon nerve stimulation at different frequencies and times of stimulation (Fig. 4C,D). Not only was the peak of the nerve-elicited tetanic contraction in mutants lower than in controls, but the fade of the mutant contractile response was more pronounced at 6 seconds stimulation than at 1.5 seconds. Thus, both the maximal amplitude and the maintenance of the contraction following nerve stimulation were greatly impaired in CLIPR-59-deficient hemi-diaphragms.

By contrast, all muscles from mutant and control embryos contracted to the same extent when directly stimulated in the presence of d-tubocurarine, which blocks neuromuscular transmission (Fig. 4E,F). This suggests that only nerve-elicited

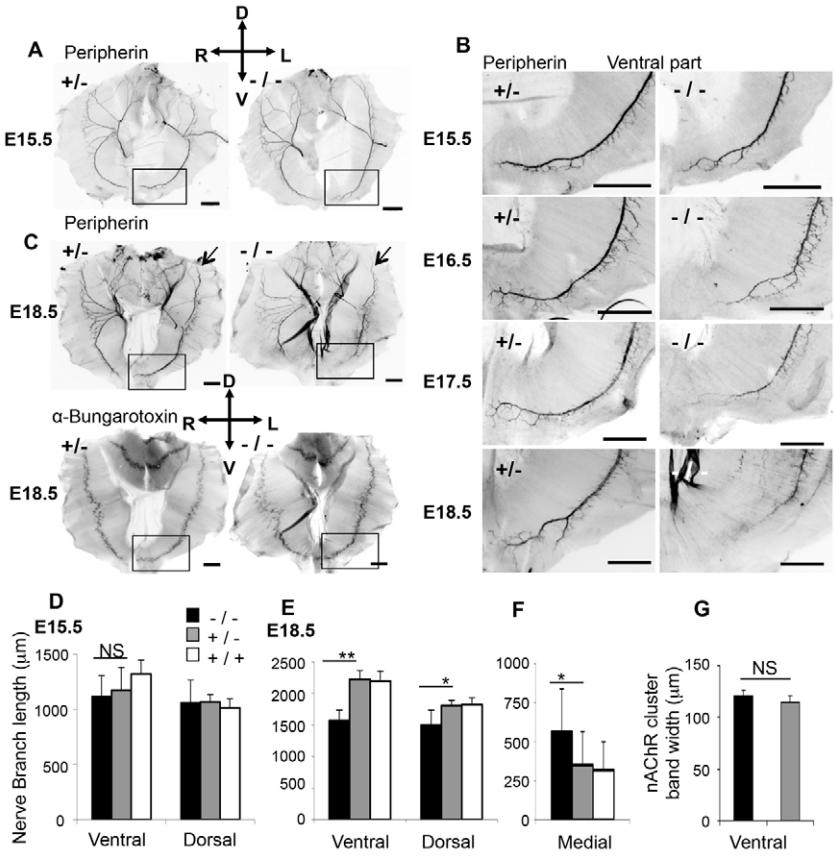

Fig. 3. Innervation of the diaphragm is impaired in *Clipr-59*$^{-/-}$ embryos from E15.5 to E18.5. Anti-peripherin and α-bungarotoxin were used to label nerve intermediate filaments and nAChRs, respectively before macroscopic imaging of diaphragm whole mounts (orientation of the diaphragm: D, dorsal; V, ventral; R, right; L, left). (**A**) The innervation patterns of the diaphragms are similar for control and mutant embryos until E15.5, as the dorsal and ventral primary branches of the phrenic nerve reach both muscle extremities. (**B**) In the absence of CLIPR-59, the innervation pattern becomes incomplete from E15.5 until E18.5, in particular in the ventral region of the diaphragm muscle. (**C**) At E18.5, both ventral and dorsal branches of phrenic nerves do not reach the most distal part of the mutant diaphragm where clusters of nAChRs are normally distributed (arrows). (**D**) At E15.5, the dorsal and ventral nerve branches in embryos of all three genotypes exhibit no significant differences in length. (**E**) At E18.5 the ventral and dorsal primary branches of the phrenic nerve are both significantly shorter in the mutant. (**F**) In the right hemi-diaphragm, the lengths of the major secondary nerve branches are longer in *Clipr-59*$^{-/-}$ mice. (**G**) In the ventral part of the left hemi-diaphragm, the band of nAChR clusters is slightly but not significantly larger in mutants. Data are means±s.e.m. *P<0.05; **P<0.001; Mann-Whitney U test. NS, non significant. Scale bars: 500 µm.

muscle contraction is altered in CLIPR-59-deficient mice, a deficiency probably caused, at least in part, by the innervation defects observed previously.

Abnormal motor innervation of other muscles in CLIPR-59-deficient mice at E18.5

To determine whether defects in muscle innervation by MN were diaphragm specific, we analyzed the innervation of other muscles in mutant embryos. Analysis of the innervation pattern of the intercostal muscles, which are also involved in breathing, did not reveal any defects in the mutant at E18.5 (data not shown). The intercostals and the diaphragm belong to different muscle classes: fast-synapsing (FaSyn) muscle and delayed-synapsing (DeSyn) muscle, respectively. These two classes of muscle exhibit intrinsically different features of focal nAChR clustering and differ in the rate at which they acquire the characteristic organization of the NMJ (Pun et al., 2002). Therefore, we next analyzed some cranial muscles, which are composed of both FaSyn and DeSyn muscles (Fig. 5A), and are innervated by branches of the facial nerve in which *Clipr-59* is highly expressed. Ear muscles are organized in two layers. The superficial layer is composed of the rostral (LALr) and caudal (LALc) parts of the levator auris longus (LAL) muscle (Fig. 5B). The deep layer is composed of interscutularis (IS), auricularis superior (AS) and abductor auricularis longus (AAL) (Fig. 5C) (Murray et al., 2010b). A dramatic loss of innervation was observed in the CLIPR-59-deficient cranial muscles at E18.5, with the extent of severity correlating to the different types of muscles (Fig. 5B,C). Again, DeSyn muscles (LALr, orange) were more affected than FaSyn muscles (LALc, red), and slow-twitch muscles (AS, blue) appeared to be relatively unaffected compared with fast-twitch (AAL, purple) muscles by CLIPR-59 deficiency. Interestingly, this tendency was already evident at E15.5 in the cranial muscles from mutant embryos (Fig. 5D), contrary to what we observed in the diaphragm at this stage (Fig. 5A). Finally, innervation defects, albeit less pronounced, were visualized in different hindlimb muscles at E18.5, suggesting that lower spinal MNs are also affected in the absence of CLIPR-59 (supplementary material Fig. S2).

Altered NMJ stability in the distal part of the phrenic nerve in CLIPR-59-deficient embryos at E18.5

To further characterize NMJ alterations, we analyzed their morphology in the diaphragm from E18.5 embryos by confocal microscopy on whole-mount preparations stained with anti-peripherin antibodies and labeled with α-bungarotoxin. Quantification of individual nAChR clusters showed that the mean surface was larger in mutant than in control E18.5 diaphragms, especially in the ventral area of the muscle (supplementary material Fig. S3A). However, the total intensity of α-bungarotoxin labeling was similar (supplementary material Fig. S3B). These results suggest that the number of post-synaptic nAChR receptors was not affected in mutant diaphragms, but their organization in clusters was perturbed in the denervated region of the mutant diaphragm. However, in this ventral region of the mutant diaphragm, the localization and levels of the muscle specific kinase MuSK, a post-synaptic protein playing a central role in the formation of NMJs, and the levels of the neural secreted agrin were unchanged compared with control diaphragms (supplementary material Fig. S4). Moreover, the proportion of innervated synapses was reduced by 30% in the ventral part of mutant diaphragms, whereas it was similar to control in the medial part where NMJs appeared to be

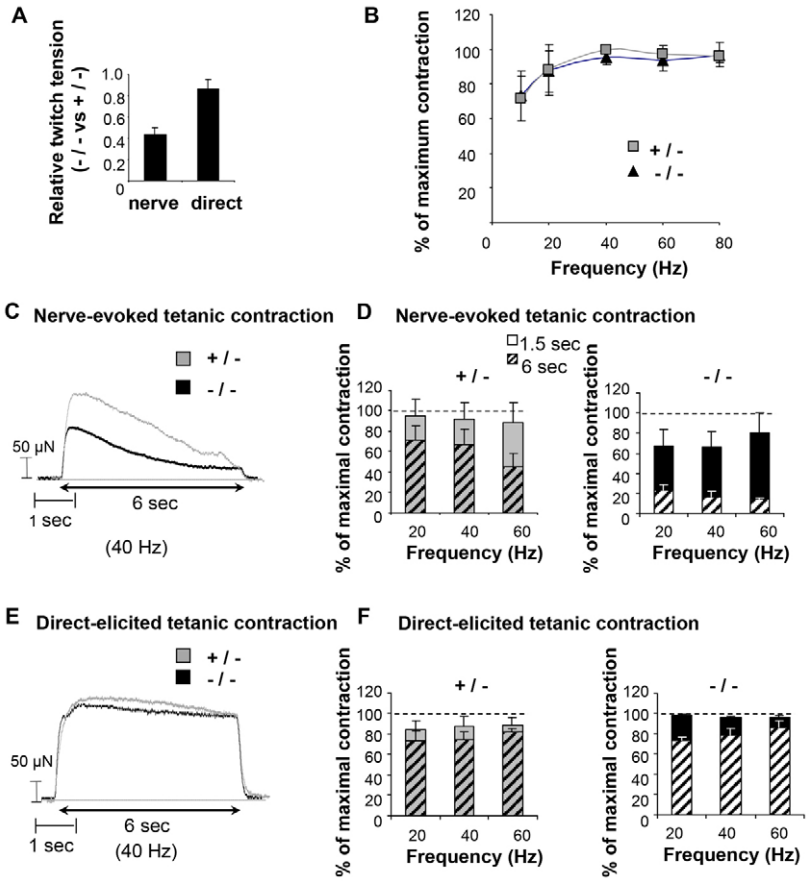

Fig. 4. The isometric contraction force of the diaphragm muscle is impaired in CLIPR-59-deficient embryos at E18.5. (**A**) In the mutant, the isometric twitch tension elicited by single nerve stimulation is markedly reduced compared with that obtained by single direct muscle stimulation. (**B**) The percentage of maximum contraction as a function of the stimulation frequency are similar in nerve-stimulated hemi-diaphragms from both control and mutant embryos. (**C**) Example of sustained tetanic contraction in diaphragms obtained by nerve stimulation at 40 Hz for 6 seconds show that the tension dropped faster in the absence of CLIPR-59 (black) than in the control (gray). (**D**) The percentage of maximal contraction is more substantially reduced for *Clipr-59*$^{-/-}$ embryos than in *Clipr-59*$^{+/-}$ embryos after 1.5 seconds of nerve stimulation (solid bars), and to an even greater extent after 6 seconds of nerve stimulation (hatched bars). (**E**) An example of the tension recording graphs obtained by a direct tetanic stimulation at 40 Hz for 6 seconds of the muscle in presence of d-tubocurarine shows that the contraction patterns for mutant (black) and control (gray) diaphragms are very similar. (**F**) The percentage of maximal contraction upon direct stimulation remains high after 1.5 and 6 seconds for diaphragms from either *Clipr-59*$^{-/-}$ or *Clipr-59*$^{+/-}$ embryos. Data are mean±s.e.m.

normal (supplementary material Fig. S3C). In both control and mutant diaphragms, presynaptic nerve terminals were observed facing the post-synaptic nAChR receptors in the core of the nerve branches (Fig. 6A, parts a and b, respectively). However, near the tip of nerve branches in mutant mice (Fig. 6Ad), the nerve frayed out and axons appeared less fasciculated and branched than in control mice (Fig. 6Ac), with shredded segments of axons (arrowhead), varicose terminals and unoccupied nAChR clusters (star).

We next examined perisynaptic Schwann cells using an anti-S-100 antibody along with a Tuj1 antibody to detect axonal tubulin (Fig. 6B). Upstream of the nerve tip, terminal Schwann cells could be observed capping NMJs in both control (Fig. 6Ba) and mutant (Fig. 6Bb) diaphragms. However at the nerve tips of mutant mice (Fig. 6Bd), axons were defasciculated, as indicated by tubulin staining (arrowhead). Schwann cells remained present and were capping the nerve terminals but their shape, identified by the presence of anti-S-100-stained membrane remnants (thick arrows in Fig. 6Bd), was slightly different than that of control Schwann cells (Fig. 6Bc). Thus, the most distal parts of the phrenic nerve in the mutant exhibited partial losses of NMJs that were probably due to axonal retraction.

An ultrastructural analysis of NMJs was performed in the ventral part of the E18.5 diaphragms where innervation defects were detected by light microscopy observations. α-Bungarotoxin was used to detect nAChRs and identify NMJs. The three main elements of the NMJ – muscle, nerve terminal (highlighted in red), terminal Schwann cells (highlighted in green) – were present even in absence of CLIPR-59. Muscle morphology looked similar between control (Fig. 7A) and mutant (Fig. 7B,C) embryos, as did the intracellular composition of the nerve terminals with numerous pre-synaptic vesicles and some mitochondria (asterisks). In both control and mutant NMJs, terminal Schwann cells were visualized capping normally the nerve terminals. However, the organization and number of nerve terminals were different. Indeed, in the ventral part of the mutant diaphragm, most junctions exhibited single or chaplets of terminals (with a mean value number of 2.5±0.4; n=41), whereas in the controls, the mean number of nerve terminals was significantly higher (mean value=5±0.7; n=67; P<0.05). Moreover, in ~10% NMJs of the mutant diaphragm, abnormal nerve terminals containing a reduced number of small clear synaptic vesicles were observed in terminals totally wrapped up in terminal Schwann cell extensions (Fig. 7D), a feature not observed in control NMJs. These may correspond to retracting nerve terminals that are being engulfed by Schwann cells. Thus, even if the tripartite composition of the NMJ was respected, nerve terminals appeared less numerous at NMJ in the ventral region of the mutant diaphragm muscle. This suggests a reduction in either the branching complexity of nerve terminals or the number of axons at NMJs in the absence of CLIPR-59.

NMJs in the ventral region of diaphragms were also imaged at E15.5 by electron microscopy (supplementary material Fig. S5). Nerve terminals (highlighted in red), capped by Schwann cells (highlighted in green), were observed in close proximity to α-bungarotoxin-labeled post-synaptic zones in both control and mutant samples (supplementary material Fig. S5Aa,Ab), indicating that NMJs were properly formed at E15.5. Figures of stacked nerve terminals were noticed at this stage in the mutant, indicating that axon terminals could branch at this stage, whereas at E18.5, mostly single terminals and chaplets of terminals were present. Strikingly,

A

	LAL rostral *	LAL caudal *	AS **	AAL **
Fiber type	Fast	Fast	Predominately slow	Fast
FaSyn/DeSyn	DeSyn	FaSyn	No data	No data

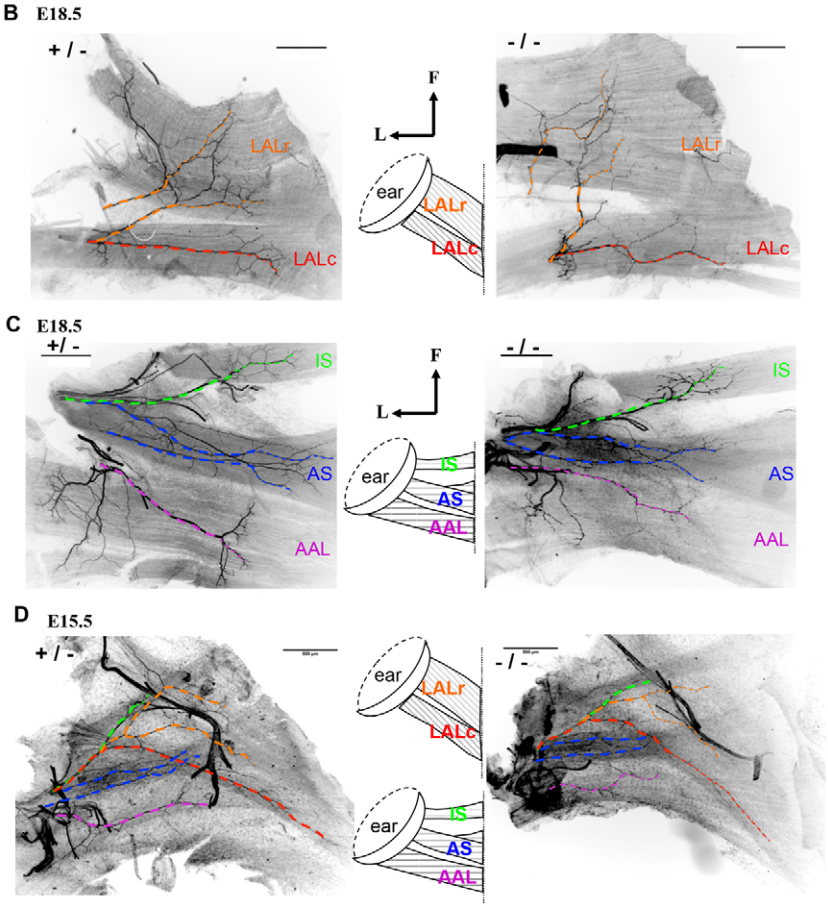

Fig. 5. Selective and premature denervation of ear muscles in *Clipr-59*$^{-/-}$ mice. Two muscle layers located between the ears of the mouse and innervated by a branch of the facial nerve were studied for innervation defects. (**A**) The properties of these ear muscles are summarized using information taken from Murray et al. [*(Murray et al., 2008); **(Murray et al., 2010b)]. (**B**) Innervation was revealed with anti-peripherin labeling, and the nerve trunk was highlighted by a color-coded broken line. The orientation of the muscles on the mouse head is indicated in the center of the figure (F, front; L, left ear). The innervation pattern of the superficial layer is severely impaired in E18.5 mutants. In particular the LALr (orange) is denervated in distal regions of the muscle, with fewer nerve branches in the mutant compared with the control, whereas the innervation of the LALc (red) is relatively normal in mutant mice. (**C**) In the muscle deep layer of E18.5 mutant, innervation is more affected in the AAL (a fast-twitch muscle, purple) with a severe axon loss and thinner axon branches than in the AS (slow-twitch muscle, blue). (**D**) Innervation defects in mutant ear muscles are already noticeable as early as E15.5, with thinner and less ramified nerve branches. Scale bars: 100 μm.

in the mutant, some nerve terminals (supplementary material Fig. S5Ad, white stars) contained fewer small clear synaptic vesicles when compared with control nerve terminals (supplementary material Fig. S5Ac), but still contained mitochondria (asterisks). Schwann cells were always present in all visualized NMJs of both mutant and control E15.5 diaphragms, and their long thin digitations were also observed facing α-bungarotoxin-labeled muscle membrane in the absence of nerve terminals, in control and mutant diaphragms (supplementary material Fig. S5Ae,f). Such immature organization was no longer observed at E18.5 (Fig. 7). These Schwann cell extensions were also detected using S-100 immunolabeling on cryosections of E15.5 diaphragms (supplementary material Fig. S5Ba,b, white arrows). No apoptotic figures were detected by TUNEL staining in S-100-positive cells imaged in cryosections of the ventral region of diaphragms from both control and mutant E15.5 embryos, confirming the ultrastructural observations.

Next, we examined whether MN cell bodies were also affected by CLIPR-59 deficiency. We counted the number of facial and spinal MNs on cervical sections in brain and spinal cord cryosections after *in situ* hybridization with an anti-peripherin probe (Fig. 8A). At E18.5, no differences in both facial and cervical MN cell body numbers were detected between mutant and control embryos (Fig. 8B). Thus, at this developmental stage in mutant embryos, there were no signs of MN loss in these two pools despite losses of innervation by the facial and spinal nerves. Consistently, immunofluorescence labeling of active caspase 3 on brain and spinal cord cryosections did not reveal any significant differences between control and mutant E18.5 embryos (data not shown). Hence, no increase in apoptosis could be observed at late developmental stages in CLIPR-59-deficient embryos.

DISCUSSION

We report here that *Clipr-59* is especially expressed in motoneuronal pools. The phenotypic and functional characterization of the innervation of different muscles in *Clipr-59* KO mouse reveals that CLIPR-59 is necessary for the stabilization of NMJs and the prevention of motor axon retraction during late embryogenesis.

Clipr-59 expression levels increase along embryonic development and MN differentiation

Clipr-59 expression in the mouse is spatially restricted, in particular to some MN pools in the brain and spinal cord. *Clip-115* mRNA and protein were also detected mostly in the brain, in particular in the inferior olive nucleus, hippocampus, cortex and cerebellum (De Zeeuw et al., 1997). In contrast, *Clip-170* expression is ubiquitous in the adult rat (Akhmanova et al., 2005).

In mouse, *Clipr-59* expression levels increase from E11.5 until birth, whereas those of *Clip-115* expression remain low from E10.5

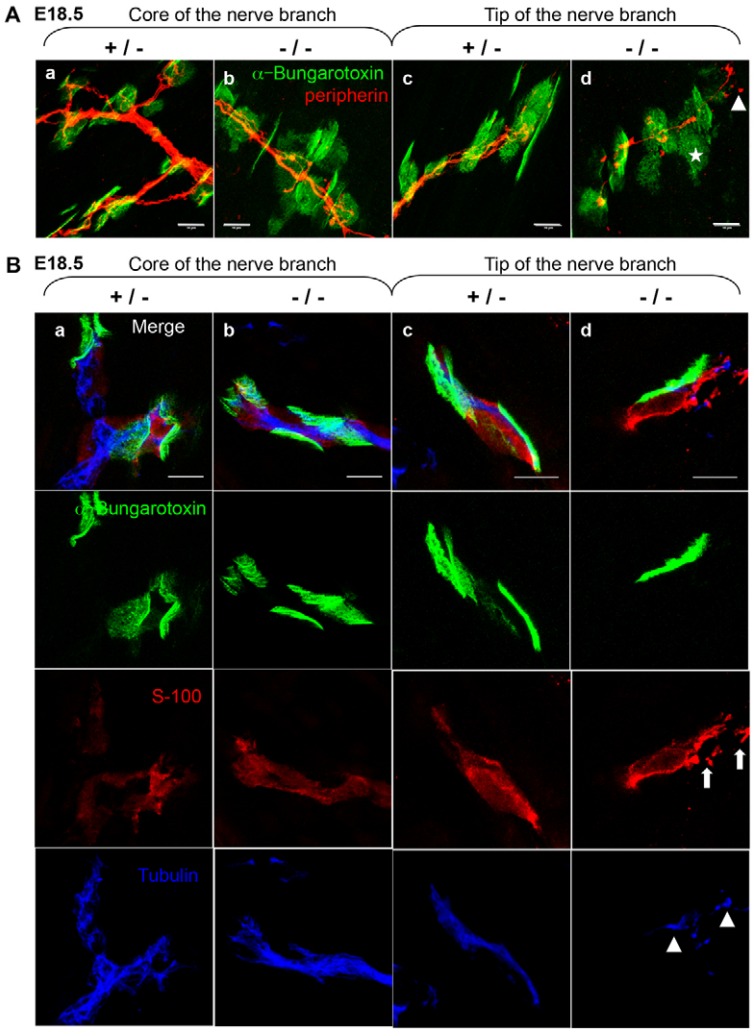

Fig. 6. NMJs appear to have formed normally but are not maintained in distal regions of the diaphragm at E18.5. (**A**) Nerve terminals and nAChRs were labeled with anti-peripherin (red) and α-bungarotoxin (green), respectively, in diaphragms and imaged by confocal microscopy. (**B**) Terminal Schwann cells were labeled with anti-S-100 (red) and neuronal tubulin was labeled with a Tuj1 antibody (blue). This series of images shows the ventral region of the left hemi-diaphragm of E18.5 embryos at the core of the nerve branch and at its end. (A) In the core of the nerve branch, normal NMJs are evident and the presynaptic nerve terminals are apposed to post-synaptic nAChRs in control (a) and mutant (b) diaphragms. At the tip of the nerve branch (c,d), the thinning of the nerve is much more pronounced in the absence of CLIPR-59 than in the control, with visible retraction bulbs (arrowhead) and uninnervated nAChRs (star). (B) S-100-positive terminal Schwann cells capping the NMJs both in control and in CLIPR-59-deficient mice. In the core of the nerve branch upstream of the nerve tip, Schwann cell morphologies are very similar in control (a) and CLIPR-59-deficient (b) diaphragms. However, at the tip of the nerve branch in CLIPR-59-deficient embryos (d), abnormally shaped Schwann cells can be observed (thick arrows) next to shedding segments of disconnected axons (arrowheads). By comparison, normally shaped Schwann cells cap healthy NMJs in control diaphragms (c). Scale bars: 10 μm.

through birth, and become very high during the first postnatal days (De Zeeuw et al., 1997). The increasing levels of *Clipr-59* expression were also observed *in vitro* in primary MN cultures from E12.5 embryos, similarly to what has been described in adipocytes (Ding and Du, 2009). Thus, *Clipr-59* expression seems to be enhanced as cell differentiation occurs and its increased expression between E12.5 and birth could be correlated with a possible role during embryogenesis. Interestingly, the temporal increase in phenotypic defects observed in *Clipr-59* KO mice between E15.5 and birth parallels the temporal normal increase in *Clipr-59* expression during development. In addition, the severity of the phenotype of KO mice could be due to the absence of functional redundancy with other CLIP members, unlike CLIP-170 and CLIP-115 (Hoogenraad et al., 2000, Komarova et al., 2002). *Clipr-59* may have appeared more recently than either *Clip-170* or *Clip-115* during evolution as it is not conserved in chicken (unlike *Clip-170* and *Clip-115*) or in mosquito (unlike *Clip-170*), but it is conserved in mammals and zebrafish.

CLIPR-59 is involved in the proper and timely maintenance of muscle motor innervation during late embryogenesis

Although CLIPR-59 deficiency is not lethal during embryonic development, mutant mice die at birth from respiratory failure. From this phenotype and the developmental expression profile of *Clipr-59* in cervical MNs, we focused on analyzing the innervation pattern of the diaphragm from E12.5, when the phrenic nerve reaches the diaphragm primordium and branches. The defects observed in diaphragm innervation could be due to axon extension defects, to axon-guidance defects or to synapse-maintenance defects. Unlike the readily apparent lack of innervation at E13.5 observed in diaphragms from mice lacking the Unc5c netrin receptor (Burgess et al., 2006), axonal projection and pathfinding by phrenic MNs appeared normal in CLIPR-59 mutants until E15.5. From E16.5 to E18.5, motor innervation became incomplete in the most distal regions of the mutant diaphragm, and phrenic branches were significantly shorter than normal. However, aneural nAChRs were still clustered in a central band that was not significantly broader in the mutant than in the control. This observation is more consistent with a retraction of pre-existing phrenic axons or a loss of synaptic connections, as occurs in neuronal neuregulin 1 mutant mice (Yang et al., 2001), than with a defect in the guidance or elaboration of the nerve.

The analyses of other muscles revealed that some facial MN projections showed similar axonal retractions, but as early as E15.5, whereas lower spinal MN projections were affected but to a less extent than phrenic MN ones at E18.5. Altogether, these different delays in the appearance of MN axon retractions parallel the time course of MN maturation along the rostrocaudal axis. It could suggest that CLIPR-59 is involved, at specific stages of embryonic

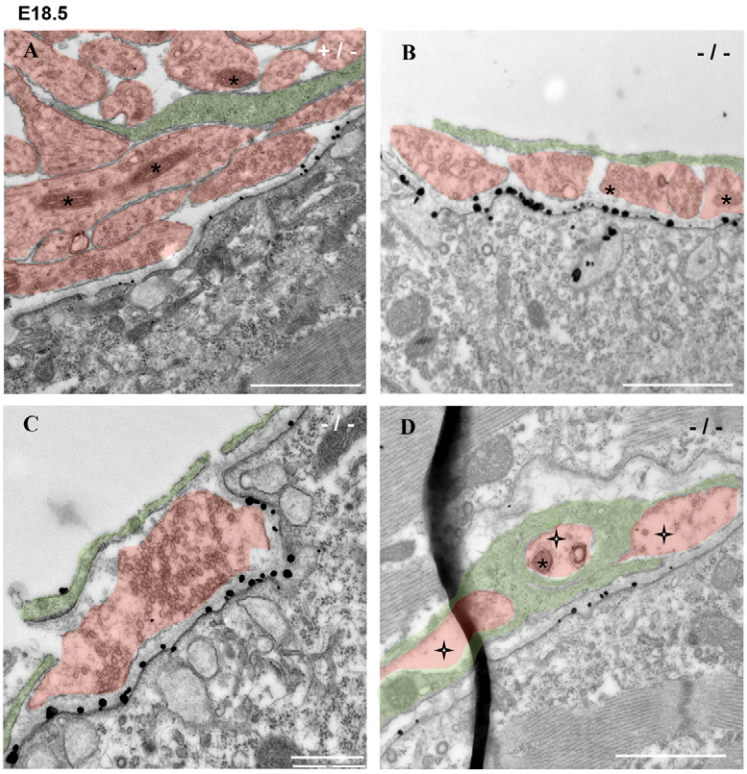

Fig. 7. The ultrastructure is modified in some NMJs of E18.5 mutant diaphragms. Presynaptic nerve terminals and terminal Schwann cells were artificially colored in light red and green, respectively. (**A**) Bundle of nerve terminals capped by a Schwann cell process in a control NMJ. Numerous pre-synaptic synaptic vesicles and some mitochondria (asterisks) are present in nerve terminals. (**B**,**C**) *Clipr-59* mutant NMJs showing either the chain-like arrangement of nerve terminals (B), or the single arrangement of the terminal (C) covered by thin Schwann cell processes. Both types of nerve terminals exhibit small clear synaptic vesicle accumulation and mitochondria. (**D**) *Clipr-59* mutant NMJ exhibiting abnormal nerve terminals (stars), totally wrapped up in Schwann cell processes containing few synaptic vesicles. Scale bars: 1 μm.

development, in the projection of MNs towards their target muscle, possibly by preventing the premature withdrawal of polyneuronal innervation. Indeed, polyneuronal innervation of diaphragm muscle fibers could represent a developmental strategy during perinatal period to allow fractional and selective recruitment of motor units as synapse elimination proceeds. In mouse, phrenic MNs are recruited as soon as E12.5 by rhythmic motor patterns generated in the spinal cord, and by E15.5 rhythmic fetal respiratory movements are already occurring (Greer and Funk, 2005). However, the influence of these synaptic inputs to phrenic MNs on trophic support or dendritic arborization during embryonic development is not yet clearly determined, and we cannot so far exclude an additional effect of CLIPR-59 deficiency on those rhythmogenic networks. As CLIPR-59 deficiency does not lead to embryonic death, the rate of NMJ innervation and activity during embryogenesis would be sufficient to ensure basic functions required for embryo survival, but the first breathing at birth could not be supported in the absence of CLIPR-59 as the near complete recruitment of diaphragm motor units would be necessary to inflate the lungs and sustain ventilation. In E18.5 *Clipr-59* mutant embryos, as in mice lacking rapsyn or agrin which are key components of NMJs involved in nAChR clustering, lower maximal nerve-induced contraction was detected in mutant diaphragms, whereas their contractile ability was not different from controls when the muscles were stimulated directly (Banks et al., 2003). Hence, the weak nerve-elicited muscle contraction is likely to be due to impaired neurotransmission in the *Clipr-59* mutant. The analysis of the present model seems to reveal a key step in MN development that would underline the strict requirement of multi-innervation maintenance during late embryogenesis until birth. Although the purpose of having a higher number of nerve terminals at the NMJs at birth than postnatally is not yet fully characterized, it will be of interest to analyze its role in the initial breathing and lung expansion at birth, and for other motor movements in newborns.

NMJs in *Clipr-59* mutants are lost distally and selectively in different skeletal muscles

In E18.5 mutant diaphragms, axons at the end of the phrenic nerve were fewer and defasciculated with shedding segments and swelling tips close to aneural nAChR clusters. These axonal structures may be representative of retraction bulbs, typically observed during axon branch removal at developing synapses. They are characterized by disorganized MT network in contrast to the typical bundling of MT in growth cones (Bishop et al., 2004; Ertürk et al., 2007). The particular morphology of the terminal Schwann cells at the tip of the phrenic nerve in mutant embryos could be due to the engulfment

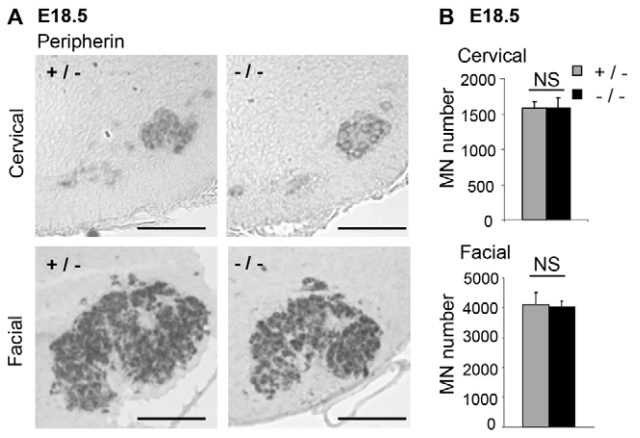

Fig. 8. The number of facial and cervical MN cell bodies is similar in control and mutant embryos at E18.5. (**A**) *In situ* hybridization with anti-peripherin probe on brain and spinal cord cryosections from E18.5 embryos. Scale bar: 100 μm. (**B**) Cell number is not significantly changed in the facial nucleus and in the cervical MN pools of mutants. Data are mean±s.e.m. NS, not significant.

of axonal membrane remnants. Ultrastructural observations of NMJs in this area of the diaphragm revealed that the number of nerve terminals was quite reduced in the absence of CLIPR-59 compared with the control, and that some nerve terminals devoid of vesicles were visualized enwrapped in Schwann cell extensions. Similar defects in some NMJs in E15.5 diaphragms, revealed at the ultrastructural but not at the macroscopic level, could be responsible for the onset of nerve terminal retraction that leads to a more pronounced phenotype of mis-innervation at E18.5. Conversely, intercostal muscles were not detectably affected in *Clipr-59*$^{-/-}$ embryos at E18.5. Similar differences in defect severity between phrenic and intercostal innervation were also observed in ErbB2- (Lin et al., 2000) and in DINE-deficient mice (Nagata et al., 2010), which could suggest that the deeper the final motor branches are into a muscle, the more severely affected the muscle innervation is. Another hypothesis is that CLIPR-59 deficiency differentially affects motor innervation according to the skeletal muscle type, such that DeSyn muscle (i.e. diaphragm, LALr) is more severely affected than FaSyn muscle (i.e. intercostals, LALc).

Indeed, we hypothesize that the expression level of CLIPR-59 may not be crucial in the selective impairment of some motor units, but could indicate the specific involvement of CLIPR-59 in these types of motor units, because of their specific physiology. Interestingly, the perinatal defects associated with CLIPR-59 deficiency are similar to the early symptoms of animals with survival of motoneuron (*SMN*) mutations (Santos and Caroni, 2003; Murray et al., 2008). Indeed, we detected no MN loss in the facial nucleus and the cervical spinal cord of *Clipr-59*$^{-/-}$ embryos at E18.5. However, E18.5 may be too early in the pathology progression to observe MN death and studying the postnatal role of CLIPR-59 in mice using inducible gene expression may resolve this issue.

Acknowledgements

We thank M. M. Portier for providing the peripherin probe; N. Galjart for the anti-CLIP-115 and -CLIP-180 antibodies; M. A. Ruegg for the anti-agrin and anti-MuSK antibodies; and S. Garel, C. Legay and G. Gacon for critical reading of the manuscript. The mouse mutant line was established at the Mouse Clinical Institute in the Targeted Mutagenesis and Transgenesis Department.

Funding

This work was supported by funding from the Association Francaise Contre les Myopathies (AFM) [14567]; by fellowships from AFM and the Association pour la Recherche sur le Cancer (ARC) [to A.C.]; and by fellowships from the Institut National de la Santé et de la Recherche Médicale (INSERM) and AFM [to N.O.].

Competing interests statement

The authors declare no competing financial interests.

Supplementary material

Supplementary material available online at
http://dev.biologists.org/lookup/suppl/doi:10.1242/dev.087106/-/DC1

References

Akhmanova, A., Mausset-Bonnefont, A. L., van Cappellen, W., Keijzer, N., Hoogenraad, C. C., Stepanova, T., Drabek, K., van der Wees, J., Mommaas, M., Onderwater, J. et al. (2005). The microtubule plus-end-tracking protein CLIP-170 associates with the spermatid manchette and is essential for spermatogenesis. *Genes Dev.* **19**, 2501-2515.

Arce, V., Garces, A., de Bovis, B., Filippi, P., Henderson, C., Pettmann, B. and deLapeyrière, O. (1999). Cardiotrophin-1 requires LIFRbeta to promote survival of mouse motoneurons purified by a novel technique. *J. Neurosci. Res.* **55**, 119-126.

Backer, S., Hidalgo-Sánchez, M., Offner, N., Portales-Casamar, E., Debant, A., Fort, P., Gauthier-Rouvière, C. and Bloch-Gallego, E. (2007). Trio controls the mature organization of neuronal clusters in the hindbrain. *J. Neurosci.* **27**, 10323-10332.

Banks, G. B., Choy, P. T., Lavidis, N. A. and Noakes, P. G. (2003). Neuromuscular synapses mediate motor axon branching and motoneuron survival during the embryonic period of programmed cell death. *Dev. Biol.* **257**, 71-84.

Bishop, D. L., Misgeld, T., Walsh, M. K., Gan, W. B. and Lichtman, J. W. (2004). Axon branch removal at developing synapses by axosome shedding. *Neuron* **44**, 651-661.

Burgess, R. W., Jucius, T. J. and Ackerman, S. L. (2006). Motor axon guidance of the mammalian trochlear and phrenic nerves: dependence on the netrin receptor Unc5c and modifier loci. *J. Neurosci.* **26**, 5756-5766.

Causeret, F., Hidalgo-Sanchez, M., Fort, P., Backer, S., Popoff, M. R., Gauthier-Rouvière, C. and Bloch-Gallego, E. (2004). Distinct roles of Rac1/Cdc42 and Rho/Rock for axon outgrowth and nucleokinesis of precerebellar neurons toward netrin 1. *Development* **131**, 2841-2852.

De Zeeuw, C. I., Hoogenraad, C. C., Goedknegt, E., Hertzberg, E., Neubauer, A., Grosveld, F. and Galjart, N. (1997). CLIP-115, a novel brain-specific cytoplasmic linker protein, mediates the localization of dendritic lamellar bodies. *Neuron* **19**, 1187-1199.

Ding, J. and Du, K. (2009). ClipR-59 interacts with Akt and regulates Akt cellular compartmentalization. *Mol. Cell. Biol.* **29**, 1459-1471.

Duprey, P. and Paulin, D. (1995). What can be learned from intermediate filament gene regulation in the mouse embryo. *Int. J. Dev. Biol.* **39**, 443-457.

Ertürk, A., Hellal, F., Enes, J. and Bradke, F. (2007). Disorganized microtubules underlie the formation of retraction bulbs and the failure of axonal regeneration. *J. Neurosci.* **27**, 9169-9180.

Grandic, M., Araoz, R., Molgo, J., Turk, T., Sepcic, K., Benoit, E. and Frangez, R. (2013). Toxicity of the synthetic polymeric 3-alkylpyridinium salt (APS3) is due to specific block of nicotinic acetylcholine receptors. *Toxicology* **303**, 25-33.

Greer, J. J. and Funk, G. D. (2005). Perinatal development of respiratory motoneurons. *Respir. Physiol. Neurobiol.* **149**, 43-61.

Hoogenraad, C. C., Akhmanova, A., Grosveld, F., De Zeeuw, C. I. and Galjart, N. (2000). Functional analysis of CLIP-115 and its binding to microtubules. *J. Cell Sci.* **113**, 2285-2297.

Hoogenraad, C. C., Koekkoek, B., Akhmanova, A., Krugers, H., Dortland, B., Miedema, M., van Alphen, A., Kistler, W. M., Jaegle, M., Koutsourakis, M. et al. (2002). Targeted mutation of Cyln2 in the Williams syndrome critical region links CLIP-115 haploinsufficiency to neurodevelopmental abnormalities in mice. *Nat. Genet.* **32**, 116-127.

Huminiecki, L., Lloyd, A. T. and Wolfe, K. H. (2003). Congruence of tissue expression profiles from gene expression atlas, SAGEmap and TissueInfo databases. *BMC Genomics* **4**, 31.

Jaworski, J., Hoogenraad, C. C. and Akhmanova, A. (2008). Microtubule plus-end tracking proteins in differentiated mammalian cells. *Int. J. Biochem. Cell Biol.* **40**, 619-637.

Komarova, Y. A., Akhmanova, A. S., Kojima, S., Galjart, N. and Borisy, G. G. (2002). Cytoplasmic linker proteins promote microtubule rescue in vivo. *J. Cell Biol.* **159**, 589-599.

Lallemand-Breitenbach, V., Quesnoit, M., Braun, V., El Marjou, A., Poüs, C., Goud, B. and Perez, F. (2004). CLIPR-59 is a lipid raft-associated protein containing a cytoskeleton-associated protein glycine-rich domain (CAP-Gly) that perturbs microtubule dynamics. *J. Biol. Chem.* **279**, 41168-41178.

Lansbergen, G., Komarova, Y., Modesti, M., Wyman, C., Hoogenraad, C. C., Goodson, H. V., Lemaitre, R. P., Drechsel, D. N., van Munster, E., Gadella, T. W., Jr et al. (2004). Conformational changes in CLIP-170 regulate its binding to microtubules and dynactin localization. *J. Cell Biol.* **166**, 1003-1014.

Leonard, D. G., Gorham, J. D., Cole, P., Greene, L. A. and Ziff, E. B. (1988). A nerve growth factor-regulated messenger RNA encodes a new intermediate filament protein. *J. Cell Biol.* **106**, 181-193.

Lin, W., Sanchez, H. B., Deerinck, T., Morris, J. K., Ellisman, M. and Lee, K. F. (2000). Aberrant development of motor axons and neuromuscular synapses in erbB2-deficient mice. *Proc. Natl. Acad. Sci. USA* **97**, 1299-1304.

Moncla, A., Landon, F., Mattei, M. G. and Portier, M. M. (1992). Chromosomal localisation of the mouse and human peripherin genes. *Genet. Res.* **59**, 125-129.

Murray, L. M., Comley, L. H., Thomson, D., Parkinson, N., Talbot, K. and Gillingwater, T. H. (2008). Selective vulnerability of motor neurons and dissociation of pre- and post-synaptic pathology at the neuromuscular junction in mouse models of spinal muscular atrophy. *Hum. Mol. Genet.* **17**, 949-962.

Murray, L. M., Gillingwater, T. H. and Parson, S. H. (2010a). Using mouse cranial muscles to investigate neuromuscular pathology in vivo. *Neuromuscul. Disord.* **20**, 740-743.

Murray, L. M., Lee, S., Bäumer, D., Parson, S. H., Talbot, K. and Gillingwater, T. H. (2010b). Pre-symptomatic development of lower motor neuron connectivity in a mouse model of severe spinal muscular atrophy. *Hum. Mol. Genet.* **19**, 420-433.

Nagata, K., Kiryu-Seo, S., Maeda, M., Yoshida, K., Morita, T. and Kiyama, H. (2010). Damage-induced neuronal endopeptidase is critical for presynaptic formation of neuromuscular junctions. *J. Neurosci.* **30**, 6954-6962.

Neukirchen, D. and Bradke, F. (2011). Cytoplasmic linker proteins regulate neuronal polarization through microtubule and growth cone dynamics. *J. Neurosci.* **31**, 1528-1538.

Perez, F., Pernet-Gallay, K., Nizak, C., Goodson, H. V., Kreis, T. E. and Goud, B. (2002). CLIPR-59, a new trans-Golgi/TGN cytoplasmic linker protein belonging to the CLIP-170 family. *J. Cell Biol.* **156**, 631-642.

Pierre, P., Scheel, J., Rickard, J. E. and Kreis, T. E. (1992). CLIP-170 links endocytic vesicles to microtubules. *Cell* **70**, 887-900.

Pun, S., Sigrist, M., Santos, A. F., Ruegg, M. A., Sanes, J. R., Jessell, T. M., Arber, S. and Caroni, P. (2002). An intrinsic distinction in neuromuscular junction assembly and maintenance in different skeletal muscles. *Neuron* **34**, 357-370.

Santos, A. F. and Caroni, P. (2003). Assembly, plasticity and selective vulnerability to disease of mouse neuromuscular junctions. *J. Neurocytol.* **32**, 849-862.

Teuling, E., van Dis, V., Wulf, P. S., Haasdijk, E. D., Akhmanova, A., Hoogenraad, C. C. and Jaarsma, D. (2008). A novel mouse model with impaired dynein/dynactin function develops amyotrophic lateral sclerosis (ALS)-like features in motor neurons and improves lifespan in SOD1-ALS mice. *Hum. Mol. Genet.* **17**, 2849-2862.

Wieland, G., Orthaus, S., Ohndorf, S., Diekmann, S. and Hemmerich, P. (2004). Functional complementation of human centromere protein A (CENP-A) by Cse4p from Saccharomyces cerevisiae. *Mol. Cell. Biol.* **24**, 6620-6630.

Yang, X., Arber, S., William, C., Li, L., Tanabe, Y., Jessell, T. M., Birchmeier, C. and Burden, S. J. (2001). Patterning of muscle acetylcholine receptor gene expression in the absence of motor innervation. *Neuron* **30**, 399-410.

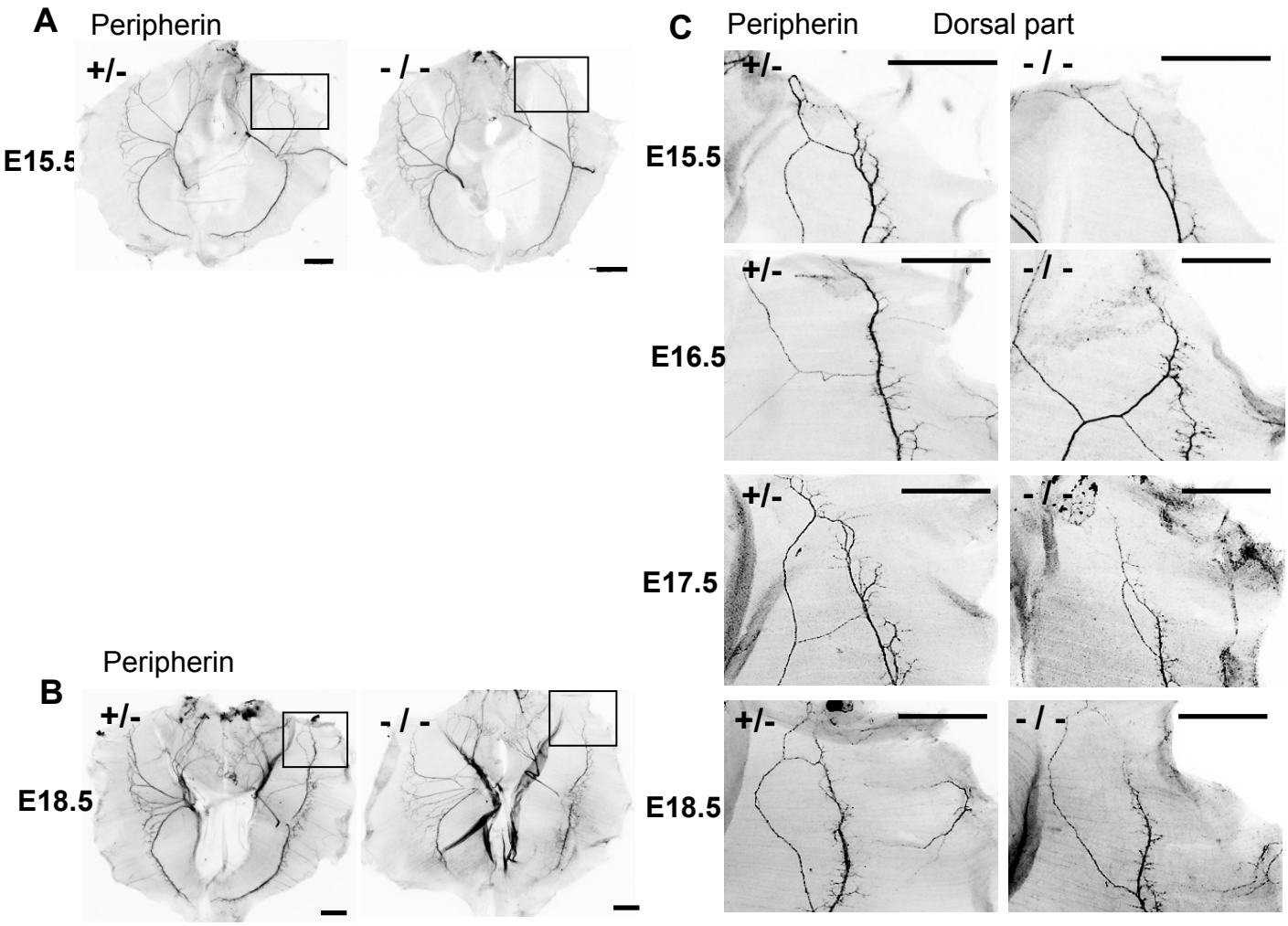

Fig. S1. Innervation of the dorsal part of the diaphragm is also impaired in *Clipr-59*$^{-/-}$ embryos from E15.5 to E18.5. Whole-mount histochemistry was performed on diaphragms using anti-peripherin to label embryonic nerve intermediate filaments and α-bungarotoxin to label nAChRs before macroscopic imaging (orientation of the diaphragm: D, dorsal; V, ventral; R, right; L, left). (**A**) The innervation patterns of the diaphragms are similar for control and for CLIPR-59-deficient embryos until E15.5, as the dorsal and ventral primary branches of the phrenic nerve reach both muscle extremities.(**B**) At E18.5, both ventral and dorsal branches of phrenic nerves do not reach the most distal part of the mutant diaphragm. (**C**) In the magnification of the dorsal region of the diaphragm muscle, the innervation pattern in the mutant becomes incomplete from E15.5 until E18.5. Scale bar: 500 μm.

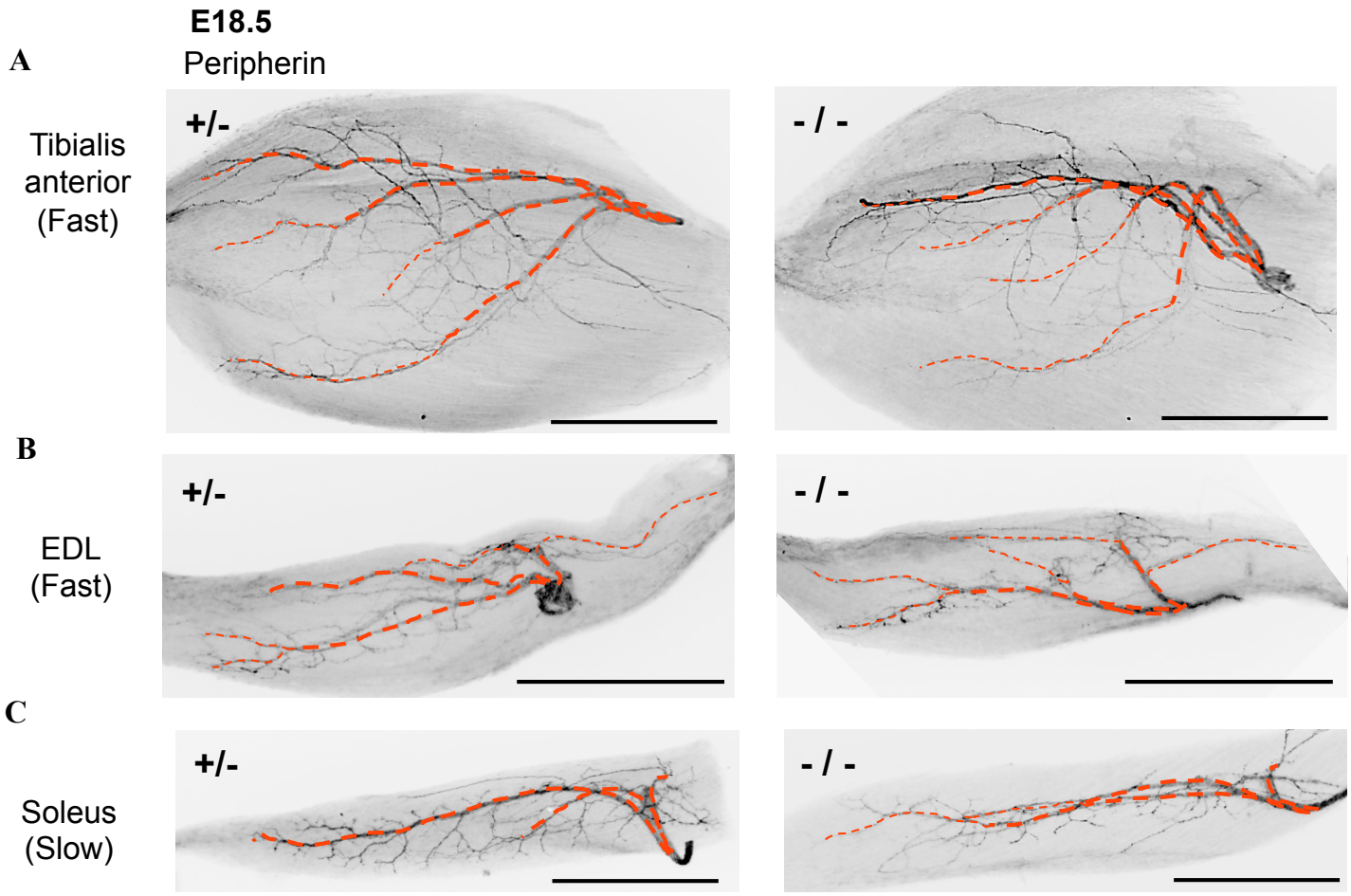

Fig. S2. Innervation defects in hindlimb muscles are less extended than in diaphragm of *Clipr-59*$^{-/-}$ embryos at E18.5. Whole-mount histochemistry was performed on dissected hindlimb muscles using anti-peripherin to label embryonic nerve intermediate filaments before macroscopic imaging. To facilitate the visualization and comparison of the innervation, the nerve trunk is highlighted by a broken red line. (**A**,**B**) In E18.5 mutant embryos, the innervation pattern is moderately altered in two fast-twitch muscles, (A) the tibialis anterior and (B) the extensor digitorum longus (EDL). (**C**) In the slow-twitch muscle soleus, only slight innervation defects can be detected in the mutant at E18.5. Scale bar: 500 µm.

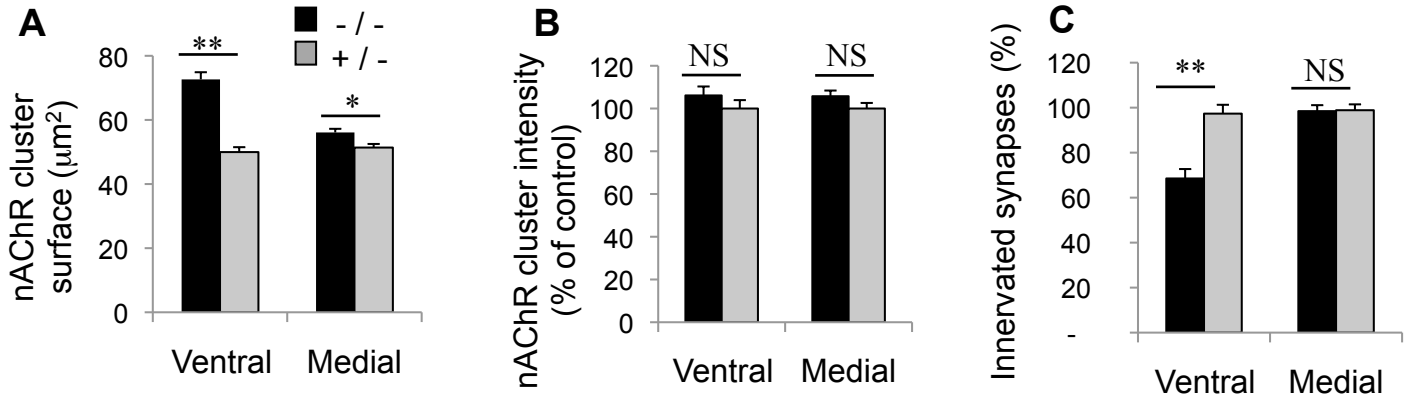

Fig. S3. Post-synaptic nAChRs are slightly less clustered in the denervated part of the mutant diaphragms at E18.5. Post-synaptic nAChRs were labeled with α-bungarotoxin in whole-mount diaphragm preparations and then imaged by confocal microscopy. (**A-C**) Measurement of (A) nAChR cluster surface, (B) α-Bungarotoxin fluorescence signal intensity and (C) percentage of innervated synapses were performed in the ventral and medial parts of the diaphragm at E18.5. Data are mean±s.e.m. *P<0.05; **P<0.001; Mann-Whitney U test. NS, non significant.

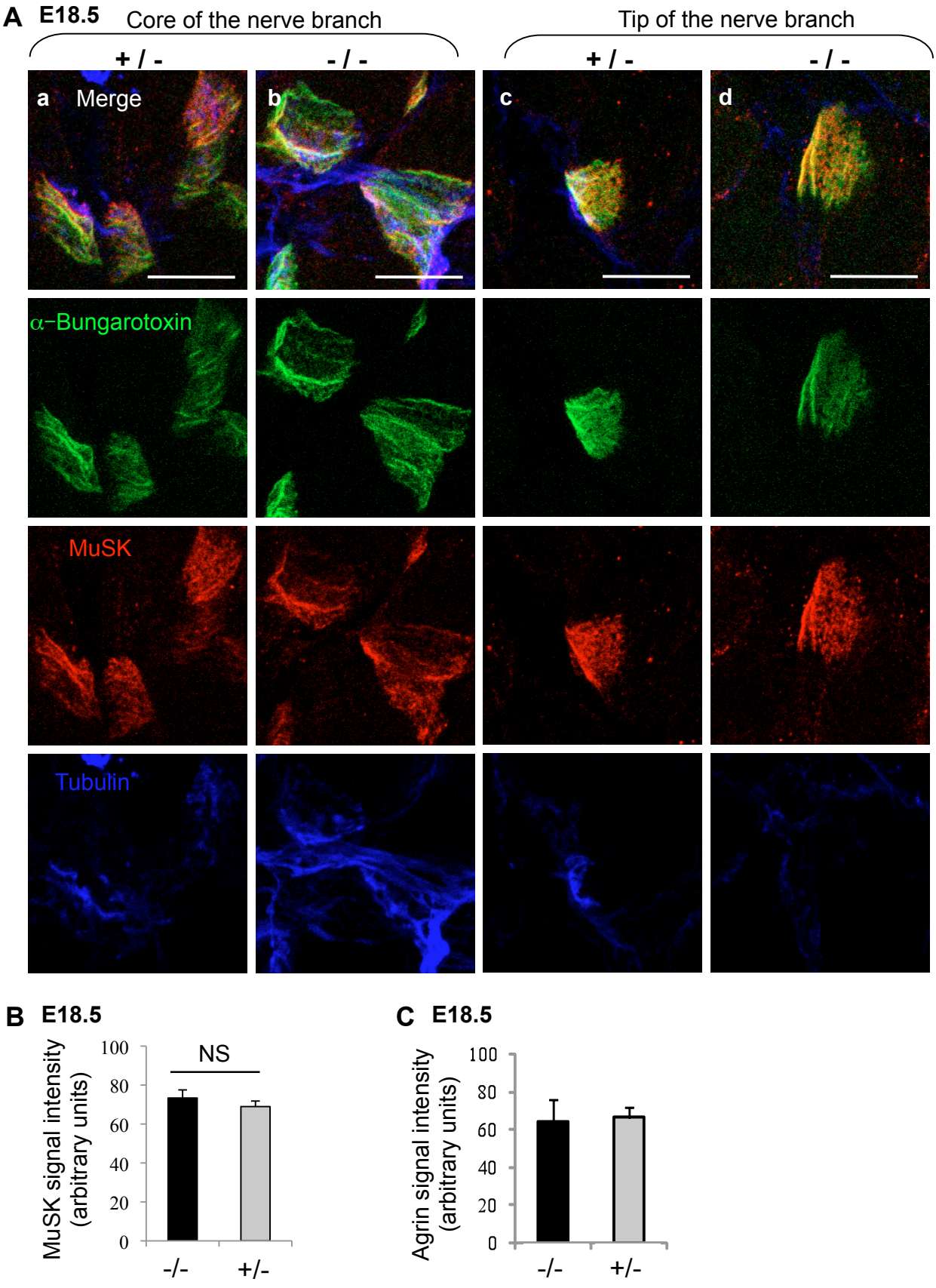

Fig. S4. Post-synaptic MuSK and neutrally secreted agrin are normally present at NMJs in E18.5 mutant diaphragms. Post-synaptic nAChRs and neuronal tubulin were labeled with α-bungarotoxin and Tuj1 antibody, respectively, and with either anti-MuSK or anti-agrin antibodies in diaphragm cryosections before imaging by confocal microscopy. (**A**) MuSK (in red) colocalized with nAChRs (in green) either at the core (a, b) or the tip (c, d) of the nerve ventral branch in both control and mutant diaphragms. (**B**,**C**) Measurement of (B) MuSK and (C) agrin fluorescent signal intensity at NMJs in the ventral part of E18.5 diaphragms. Data are mean±s.e.m. Mann-Whitney U test. NS, non-significant. Scale bar: 10 µm.

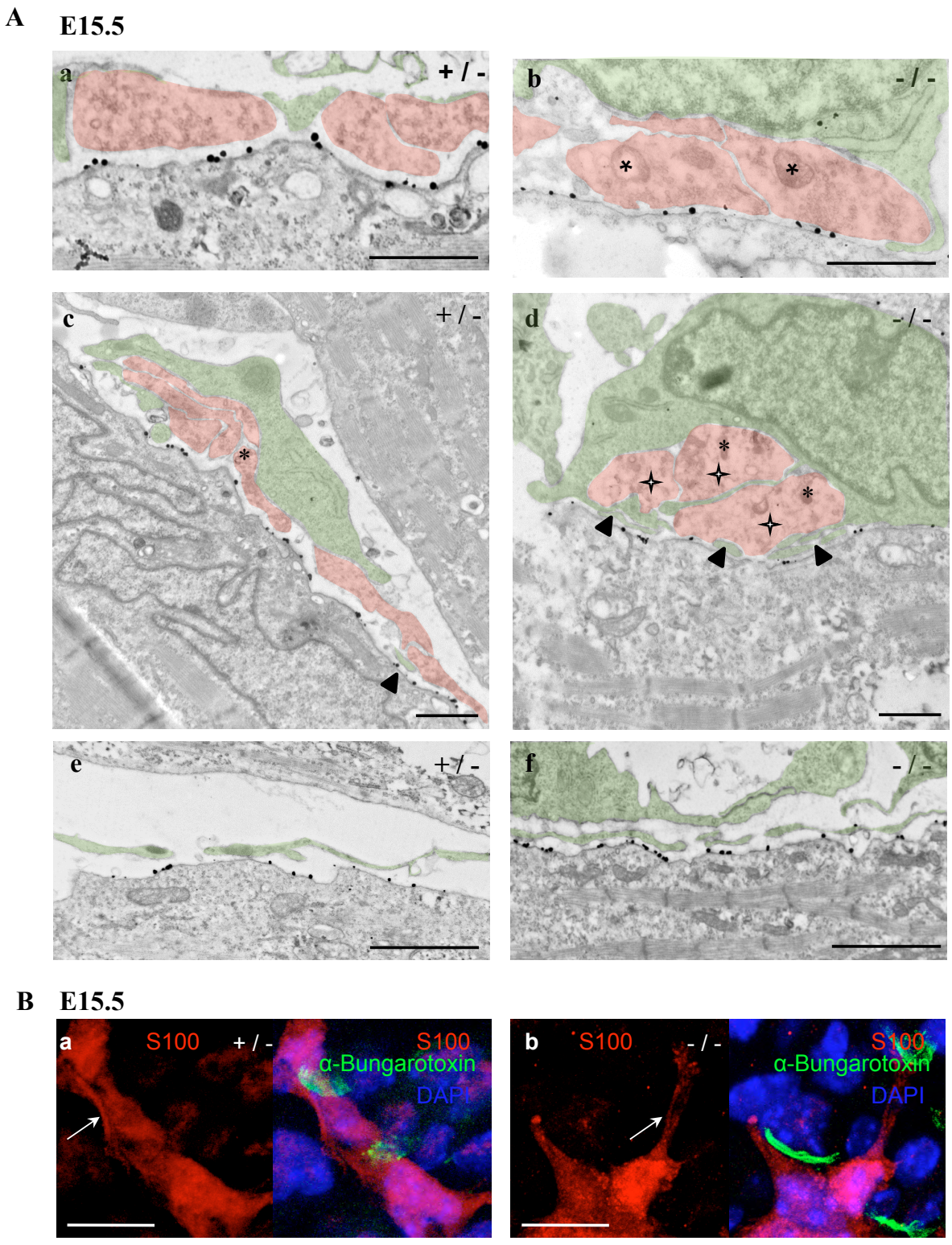

Fig. S5. At E15.5, some defects are already apparent at the ultrastructural level in few NMJs in the ventral part of mutant diaphragm muscle. (**A**) Longitudinal ultrathin sections were cut through muscle fibers of the ventral region of diaphragm of E15.5 embryos. NMJs were detected by labeling nAChRs with biotinylated α-bungarotoxin and streptavidin coupled to gold particles. Presynaptic nerve terminals and terminal Schwann cells are artificially colored in light red and green, respectively. In both control and mutant diaphragms, nerve terminals containing pre-synaptic vesicles and mitochondria (asterisks), and capped by large Schwann cells are observed at NMJ (a, b). However, in *Clipr-59* mutant, in some NMJs (stars in d) the nerve terminal composition appeared abnormal with few vesicles accumulating (but still some mitochondria, asterisks). The presence of Schwann cell processes in the synaptic cleft between presynaptic and post-synaptic components (arrowhead), and enwrapping nerve terminals could suggest their engulfment by Schwann cells. These Schwann digitations were observed to a lower extent in the synaptic cleft of some NMJs of control samples (c), and also in regions devoid of nerve terminals (d and e). (**B**) Using anti-S-100 antibody on E15.5 diaphragm cryosections, similar Schwann extensions were evidenced (arrow) by light microscopy in both control and mutant samples (a and b, respectively). Scale bars: 1 µm in A; 10 µm B.